A Fuzzy Logic Controller Based MPPT Technique for Photovoltaic Generation System

Walid S. E. Abdellatif[1, 4], Mohamed Saad Mohamed[2], Shimaa Barakat[2], and Ayman Brisha[3]

[1]Electrical Dept., Faculty of Technology and Education, Suez University, Suez, Egypt.
[2]Process Control Technology Dept., Faculty of Technology and Education, Beni-Suef University, Beni-Suef, Egypt.
[3]Electronics Dept., Faculty of Technology and Education, Beni-Suef University, Beni-Suef, Egypt.
[4]Department of Electronics and Electrical Communications Engineering, Higher Institute of Engineering and Technology – Kafr Elsheikh, Egypt.
walid.abdellatif@suezuniv.edu.eg, Msm19932018@gmail.com, shimaabara@yahoo.com, and, abrisha@techedu.bsu.edu.eg

Abstract: Solar energy is abundant and sustainable energy that photovoltaic (PV) cells can transform directly into electricity. Several conditions such as temperature and solar irradiance, influence the power production of PV systems. Maximum power point tracking (MPPT) methods have been developed and used in PV systems to improve productivity due to changing weather conditions. This paper addresses the modeling and simulation of MPPT of a grid-connected PV system with the aid of a fuzzy logic controller (FLC). FLC results compared with Perturb & Observe (P&O) algorithm and incremental conductance (IC). A simulation toolbox MATLAB Simulink was used to validate the findings experimentally. The performance of the suggested MPPT FLC indicates that the FLC reaches the optimum power point more effectively than traditional approaches.

Keywords: maximum power point tracking, photovoltaic, Fuzzy logic controller, incremental conductance, perturbation and observation.

1. Introduction

Owing to the ongoing depletion of conventional fuels and petroleum resources, renewable energy is in high demand. Solar energy has become one of the best clean energy options among the available renewable energy sources and is seen as a better substitute for traditional energy. Solar power harvest has played a crucial role in fulfilling electricity demand over the last decade. Furthermore, various researchers have been attracted to suggest studies for this field on the enriched size and environmentally sustainable nature of solar energy. The output PV system's nonlinear characteristics involve the maximum power point (MPP) operation. Control algorithms are needed to ensure MPP operation at any moment of solar and ambient temperature. The challenge is to get the lowest operating point oscillation MPP [1].

In recent decades, various research activity on MPPT for solar PV systems has been conducted and the approaches developed so far can be narrowly categorized into traditional and soft computing methods. Incremental Conductance (IC) [2]–[6], Perturb and Observe (P&O) [7]–[11], Hill Climbing (HC) [12]–[16] and Global [17]–[19] MPPT methods are classified as traditional methods. Where these approaches are able of monitoring maximum power just during uniform irradiation but struggle when partial shading exists. These approaches often demonstrate weak convergence, poor tracking speed, and significant steady-state oscillatory [20], [21]. For better results, traditional methods need to merge with other methods to detect MPP under partial shading conditions. Thanks to the numerous advantages such as their ability to tackle non-linearity, broad search speed exploration, and coherent ability to reach global optimum areas, soft computing methods are considered a prime alternative for non-linear optimization. MPPT soft computation approaches are Artificial Neural Network (ANN) [22]–[24], Fuzzy Logic Control (FLC) [22]–[24], in addition to heuristic and met heuristic algorithms [25]–[29]. Of the soft computing approaches, ANN and FLC are information-based structures that involve

Received: February 12th, 2021. Accepted: June 17th, 2021
DOI: 10.15676/ijeei.2020.13.2.9

comprehensive knowledge when applying the algorithm. ANN and Fuzzy Logic are successful in tracking MPP but need a significant amount of memory for training and applying rules. This paper proposes an efficient and usable control system based on the FLC method to achieve the MPPT from PV system under different conditions. FLC is studied under various conditions of differing temperature, solar irradiance values. The main contribution of this paper is the practical and mathematical investigation of the proposed method. Besides, a thorough comparison is made between the application of the proposed control method and the P&O, and IC methods to illustrate the effectiveness of the proposed system.

The paper is presented as follows: the next section includes the mathematical model of the PV, the boost converter, and the interface of the grid inverter controller respectively. The principles of the P&O, IC, and FLC techniques have been well described in section III. Section IV analyzes the results obtained from the simulation. While sections V and VI demonstrate the experimental setup of on-grid PV systems and the experimental results respectively. The conclusion has been drawn in the last section.

2. System Description

Figure 1 illustrates the schematic diagram for the three-phase system associated with PV generation. The suggestion system comprises of two sections, the first section incorporates a PV array, DC link capacitor, boost converter, three-stage inverter, RL filter, step-up transformer, and the three-stage utility grid. The subsequent section is the control part MPPT by utilizing diverse MPPT methods and the inverter controller with a three-phase PV grid associated system.

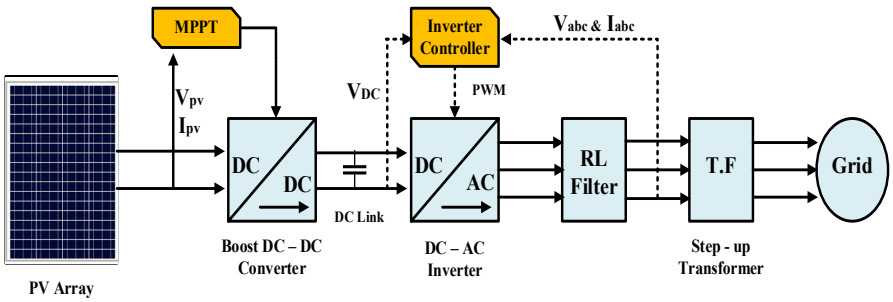

Figure 1. Simplified diagram of grid-connected of the PV system

A. PV Modeling

Due to its balance between precision and simplicity in various implementations, the single diode PV equivalent device model is one of the most commonly embraced [30]. Figure 2 displays a single-diode equivalent circuit of a PV solar cell. Figure 3(a) and (b) showed the I-V and P-V characteristics under variable irradiation of the studied PV module.

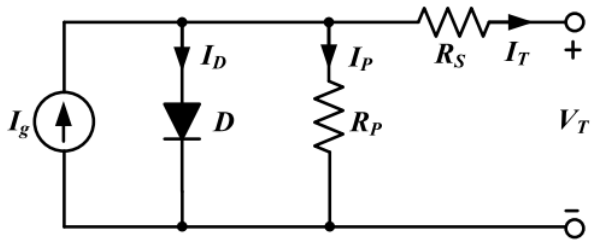

Figure 2. Single-diode equivalent circuit of a PV cell.

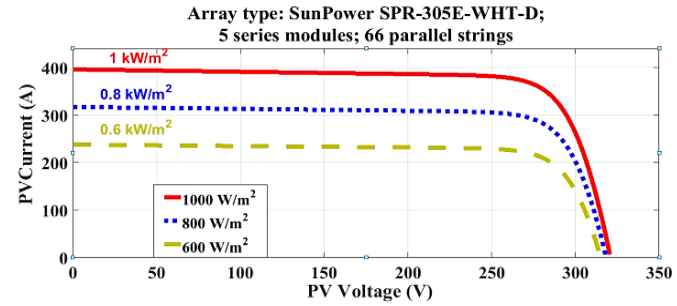

(a)

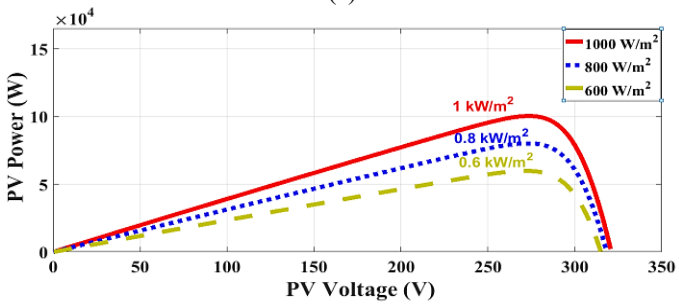

(b)

Figure 3. (a) I-V and (b) P-V characteristics curves under variable irradiation.

The following series of equations will describe the mathematical model of the I-V characteristics [31]:

$$I = I_s \left[e^{V_d / nV_s} - 1 \right] \quad (1)$$

$$I = I_1 - I_d \quad (2)$$

$$I = I_{ph} - I_o \left[e^{\left(V + R_s I / V_T \right)} - 1 \right] - \frac{V + R_s I}{R_p} \quad (3)$$

$$I = n_p I_{ph} - n_p I_{rs} \left[\exp\left(\frac{qv}{KTAn_S} \right) - 1 \right] \quad (4)$$

Where, I is the cell current, I_1 is the current directly proportional to the sun irradiation, I_d is the normal diode current, I_{ph} is photocurrent, I_o is reverse saturation current, V is Cell voltage, R_s is Series resistance, R_p is Parallel resistance, V_T is Thermal voltage, n_S is the number of cells in series, n_p is the number of cells in parallel, q charge of an electron, K is Boltzmann's constant, A is p-n junction ideality factor, T is cell temperature, I_{rs} is the cell reverse saturation current.

B. Boost Converter Modelling

As the adaptation state (between PV generator and load) happens, a basic DC-DC boost converter diverts the power consumption from the PV generator and the load. An acceptable duty signal of (0<D<1) characterizes the adaptation. The PWM signal regulates the IGBT valve gate in the boost converter [32]. Figure 4 displays the DC-DC boost wiring Simulink diagram.

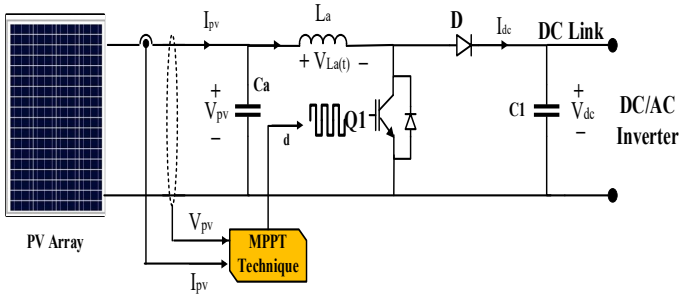

Figure 4. The basic configuration of the DC/DC boost converter

$$V_o = V_{in}/(1-D) \quad (5)$$

$$I_{out} = (1-D)I_{in} \quad (6)$$

$$R_{eq} = R_{in}(1-D)^2 \quad (7)$$

$$R_{in} = V_{in}/I_{in} = R_O(1-D)^2 \rightarrow D = 1-\sqrt{\frac{R_{in}}{R_O}} \quad (8)$$

$$L = \frac{(V_o - V_{in})V_{in}}{f(\Delta I)V_O} \quad (9)$$

$$C = \frac{(V_o - V_{in})I_{out}}{f(\Delta I)V_O} \quad (10)$$

Where, V_o is the output voltage, V_{in} is the input voltage, D is the duty cycle, I_{out} is output current, I_{in} is input current, R_{eq} is the equivalent resistance of the DC-DC boost converter, R_{in} is input resistance, R_o is the output resistance of the PV system, L is the Inductor of the DC-DC boost converter, C is a capacitor of the DC-DC boost converter, f is the frequency, ΔI is the current ripple, ΔV is voltage ripple.

C. The interface of the grid inverter controller

To supply electricity from the PV-array part to the power grid, the grid-connected inverter is used. DC bus voltage regulation and controlling active and reactive power transmitted to the grid are managed by the converter under various climatic conditions. A Unity Power Factor (UPF) procedure is implemented by the insertion into the grid of zero reactive currents. In Figure 5, the control block diagram is shown. The internal control loops use two PI controllers to modify the direct and quadrature currents. For DC-voltage to meet reference one, V_{dc_ref} the external PI controller loop is used [33].

The general relation between the grid-connected inverter voltages and line currents can be described as:

$$\begin{bmatrix} Ea \\ Eb \\ Ec \end{bmatrix} = Rf.\begin{bmatrix} ia \\ ib \\ ic \end{bmatrix} + Lf.\,{}^{d}/_{dt}\begin{bmatrix} ia \\ ib \\ ic \end{bmatrix} + \begin{bmatrix} va \\ vb \\ vc \end{bmatrix} \quad (11)$$

Where, va, vb and vc are the voltages of the grid, Ea, E_b, and Ec are the output of inverter voltages, R_f, is the filter resistance, L_f is the filter inductance and ia, ib and ic are the line currents of the grid.

The rotation reference frame synchronized with the grid voltage vectors is defined as [33]:

$$V_q = e_q - i_q.R_f - L_f.\,{}^{di_q}/_{dt} - .i_d.L_f \quad (12)$$

$$V_d = e_d - i_d.R_f - L_f.\,{}^{di_d}/_{dt} - \omega.iq.L_f \quad (13)$$

Where, iq and id are the injected grid currents of q-axis and d-axis, e_q and e_d are the voltage of the inverter of q-axis and d-axis,V_d, V_q are the voltage of the grid d-axis and q-axis and ω is the angular frequency of the grid.

Instantaneous active and reactive power outputs are computed as follows [34]:

$$Q = \frac{3}{2}\left[i_q . V_d - i_d . V_q\right] \quad (14)$$

$$P = \frac{3}{2}\left[i_d . V_d - i_q . V_q\right] \quad (15)$$

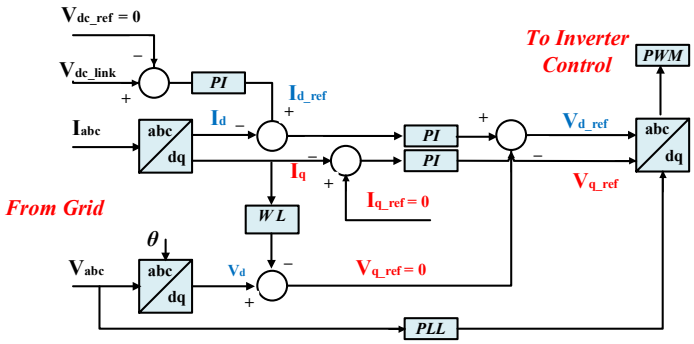

Figure 5. Block diagram of the Inverter control.

3. MPPT Techniques

A. Incremental Conductance (IC) Technique

Incremental Conductance MPPT approach uses PV source current and voltage to locate PV panel MPP. It incorporates the concept of the optimum feature when its slope is zero [33]. The IC MPPT flow chart is shown in Figure 6. Comparing the IC $\partial I/\partial V$ will track the MPP to the instantaneous one I/V as defined in equations (16-18) [35]:

$\partial I/\partial V=0$ at MPP (16)

$\partial I/\partial V< -I/V$ at the right hand of MPP (17)

$\partial I/\partial V> -I/V$ at the left hand of MPP (18)

B. Perturb and Observe (P&O) Technique

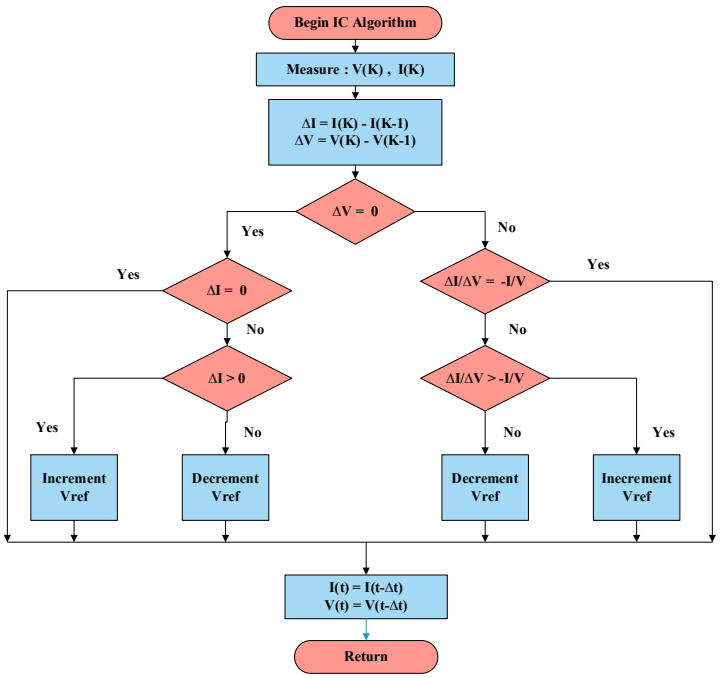

Figure 6. IC algorithm flowchart.

The P&O technique is often used to track MPP under consistent meteorological conditions (ambient irradiation and temperature) due to its simplicity of implementation. This procedure may be used to operate on PV voltage accompanied by another control block or immediately on the DC/DC converter's duty cycle. The P&O technique is focused on the disturbance of the duty cycle or voltage and the detection of the sign of power variance as a feature of voltage variation, as represented in the flow chart shown in Figure 7.

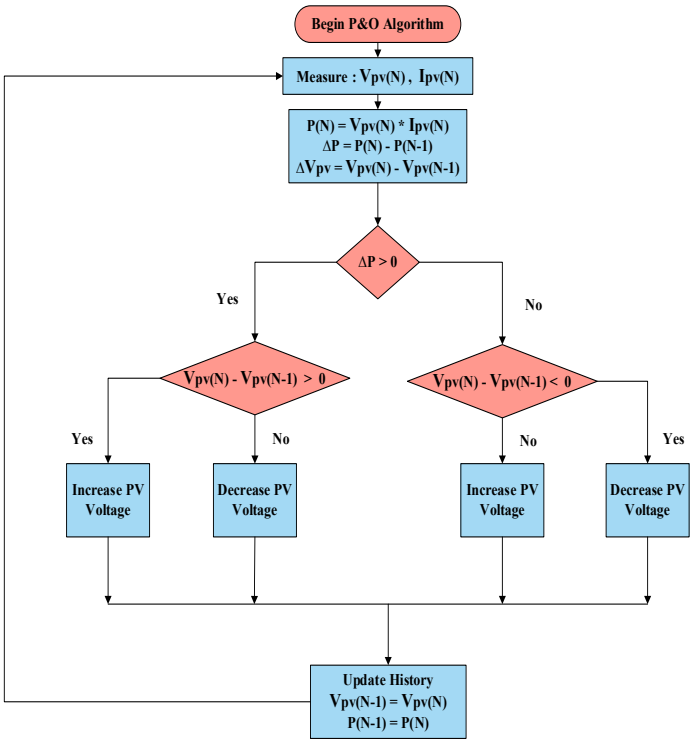

Figure 7. P&O algorithm flowchart.

C. Fuzzy Logic Controller (FLC)Technique

When using conventional controls, we need to know about the configuration and objective feature identified in specific terms. So, in different situations, it becomes really difficult to use. One may add human expertise and knowledge to construct the controller by employing fuzzy reasoning to control it. If-Then guidelines are used for the design of a controller that are known as control rules [36]. A fuzzy-logic controller is used to control the operation of a buck-boost converter. FLC runs using the 'Mamdani' technique [37]. After computing, fuzzy values are converted into crisp values utilizing a defuzzification procedure [38].

In FLC coupled inputs, the first is 'error' which is the discrepancy achieved by differentiating the output voltage and the reference value, whereas the second input is 'change error' which is a time-related error. 'Duty ratio' is the gain from the fuzzy-logic controller [39].

As shown in Figure 8, FLC consists, generally, of three parts: 1) fuzzification, 2) knowledge base (fuzzy rule base, data base), 3) defuzzification. In the fuzzication process, the input crisp values are converted to fuzzy values, which are realized by linguistic variables, e.g., high, big, medium, slow etc. The fuzzy rules are based on a set of rules, which depend on IF–THEN rule [40]. As conducted in Table 1, the required signals are based on 25 rules of matrix inference, where the membership function determines the relevance between these rules. NB, NS, EZ, PS and PB are abbreviations for Negative-Big, Negative-Small, Equal-Zero, Positive-small and Positive-Big, respectively. The FLC algorithm flowchart shows in Figure 9.

The rule base is constructed by utilizing linguistic functions as in Table 1. The FLC principles are used to describe 'If' and then' relations. Calculations are carried out using the fuzzy interaction mechanism that is the controller's brain. After that there is a defuzzification procedure in which fuzzy values are transformed to narrow values [40].

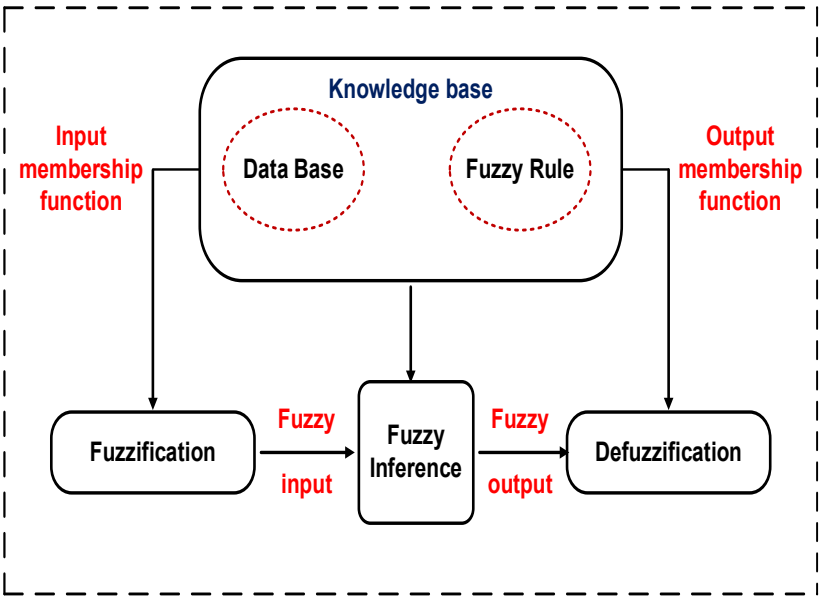

Figure 8. Fuzzy MPPT structure.

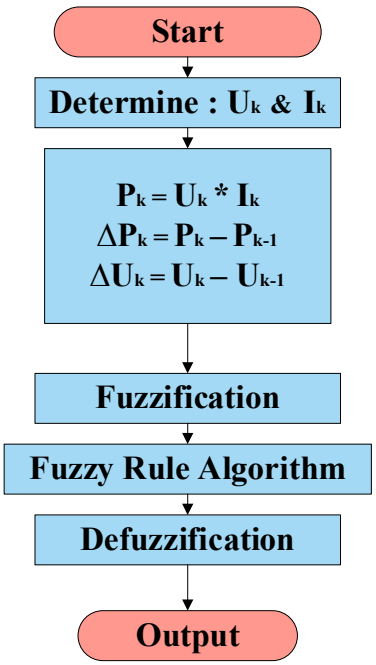

Figure 9. FLC algorithm flowchart.

Table 1. Fuzzy rules

E	CE				
	NB	NS	ZO	PS	PB
NB	ZO	ZO	NB	NB	NB
NS	ZO	ZO	NS	NS	NS
ZO	NS	ZO	ZO	ZO	PS
PS	PS	PS	PS	ZO	ZO
PB	PB	PB	PB	ZO	ZO

4. Results and Discussion

A. Results under step changes of solar radiation

MATLAB processing condition is utilized to show the proposed method of legitimacy on the PV network associated framework. The framework specifics are indicated in Table 2. Figure 10 display the difference in sun-oriented radiation under the step profile with the steady surrounding temperature, as sun-powered radiation beginning from 1000 W/m^2 was step by step decrease radiation to 800 W/m^2 and afterward decrease radiation until 600 W/m^2. At long last come back to 800 W/m^2. Figure 14 shows, PV yield framework execution correlation with IC, P&O, and FLC technique under step variations of sunlight-based radiation. The yield of PV energy, in the three various procedures, displays that the best yield power utilizing the FLC strategy contrasted with another strategy IC and P&O method. Additionally, by contrasting the FLC technique execution and traditional P&O in the quick-shifting climate situations of sun-based radiation, the FLC is more accurate than the traditional strategy and under the high efficiency, quick-shifting climate sun based radiation conditions. The FLC keeps track of the optimum MPPT. The suggested FLC technique for following the framework builds productivity than traditional methods [21].

Table 2. PV System parameters

Parameters	Values	Parameters	Values
Maximum Power (W)	305.226 W	Capacitance Of Boost Converter	100 µF
Current At Maximum Power Point Imp (A)	5.58 A	Resistance Of Boost Converter	0.005 Ω
Voltage At Maximum Power Point Vmp (V)	54.7 V	Inductance Of Boost Converter	5 MH
Open Circuit Voltage Voc (V)	64.2 V	Converter Switching Frequency	10 kHz
Short-Circuit Current Isc (A)	5.96 A	Dc Link Reference Voltage	500 V
Parallel Strings	66	Inductance Of FILTER	0.25 MH
Series-Connected Modules Per String	5	Resistance Of FILTER	0.015 Ω
Step Up Transformer	260V/ 25 KV	Grid Frequency	60 HZ
Grid Voltage	25 kV		

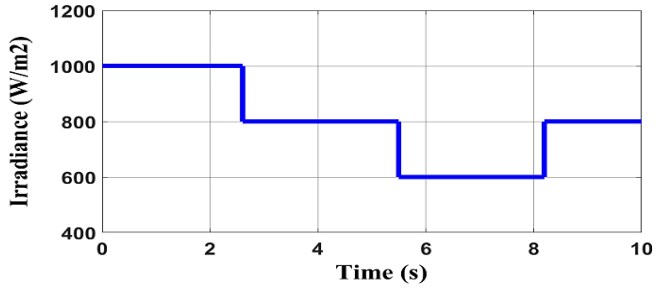

Figure 10. Irradiance is a step changed profile.

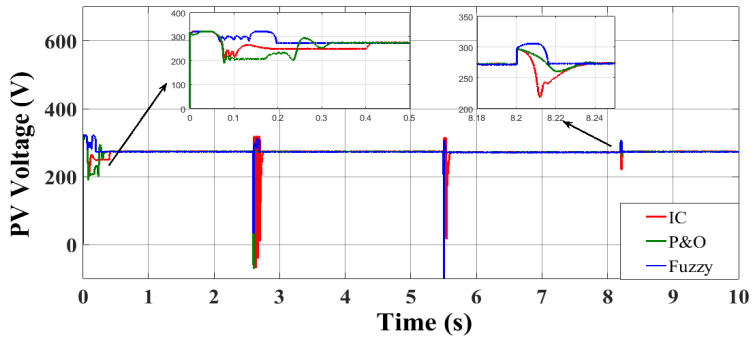

(a)

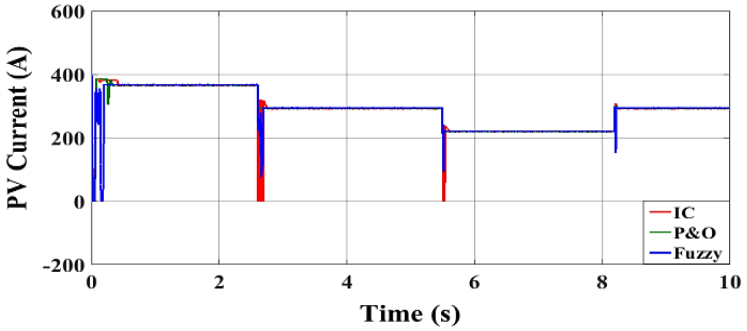

(b)

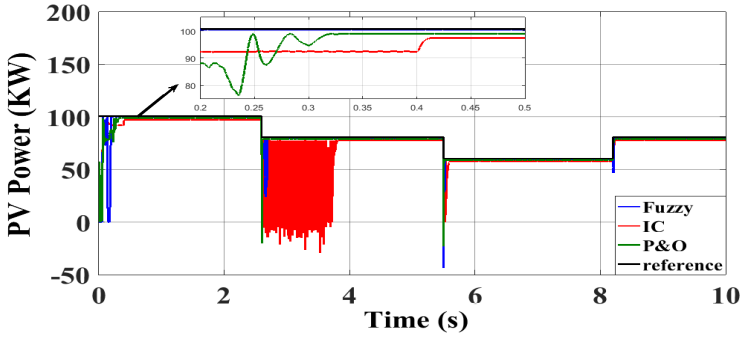

(c)

Figure 11. Performance comparison of PV system under step change irradiance; (a) output of PV voltage (b) output of PV current, and (c) output of PV power.

The PV voltage with FLC is constant with variation from solar radiation as shows in Figure 11 (a) , by contrasting of yield the PV current of the three strategies as clarified in Figure 11(b), the FLC strategy is the most ideal exhibition to follow the limit of PV current. Figure 11 (c) displays the PV power in the three various strategies, demonstrating that the best yield power utilizing FLC compared to another technique IC and P&O. The framework motions are decreased about the MPP and the framework reaction is lower than the IC and P&O algorithm. Table 3 displays the PV power under various radiation between three various methods. And good agreement between the PV powers with the ideal or reference condition and PV current with solar radiation profile. As consequence the MPPT with controller is achieved, but the FLC is the best and fastest response to the sudden change of radiation compared to the IC and P&O algorithm as shows in Figure 11 and 12.

Table 3. PV output power under different radiation

Time (sec)	Solar Radiation (W/m^2)	PV Output power (KW)		
		IC MPPT	P&O MPPT	Fuzzy MPPT
1 to 2.6	1000	97.32	98.84	100.38
2.6 to 5.5	800	77.73	78.93	80.17
5.5 to 8.2	600	58.06	58.96	59.87
8.2 to 10	800	77.73	78.93	80.17

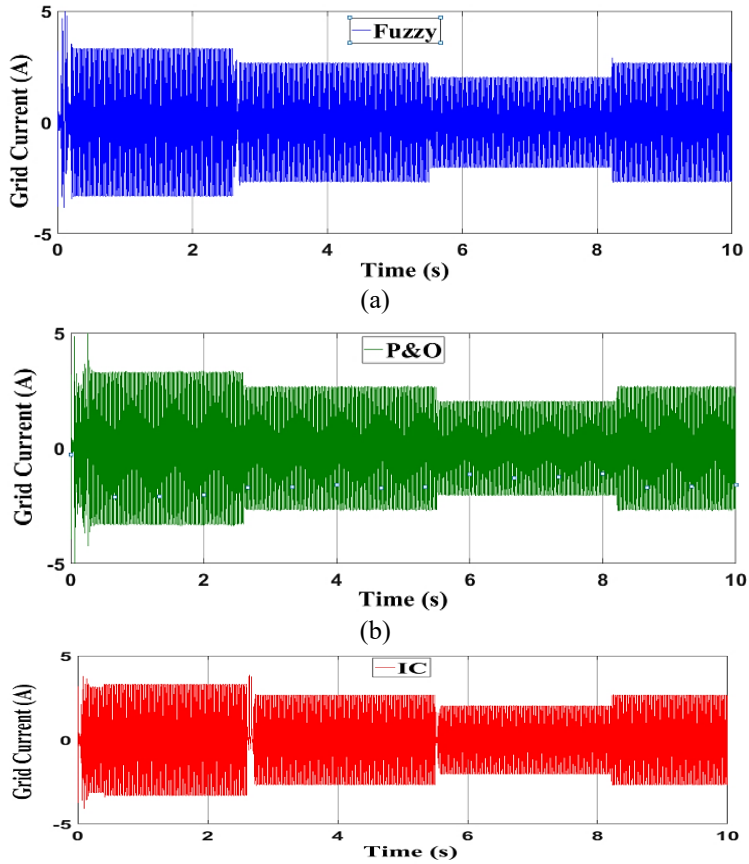

Figure 12. Grid current under different algorithms.

Figure 12, Figure 13, and Figure 14, illustrates the response of the grid voltage, current, and power to the different methods that were used to achieve the maximum value of the output power of the PV system at different solar radiation conditions. The framework shows a portion of the fundamental consequences of the utility grid currents, voltages, and powers and that the framework has coincided with the utility grid. The grid voltage and current at single-phase utilizing FLC, IC, and P&O techniques under step variations of radiation as appeared in Figure 12 and Figure 13. The outcomes present that the voltage is steady to keep up the concurrence of the utility grid; likewise, the grid current is varied to keep track of the highest current. To guarantee the activity of the unit power factor, the reactive power rate must be zero. Table 4 and Figure 14, displays the grid output power under different radiation between three various methods.

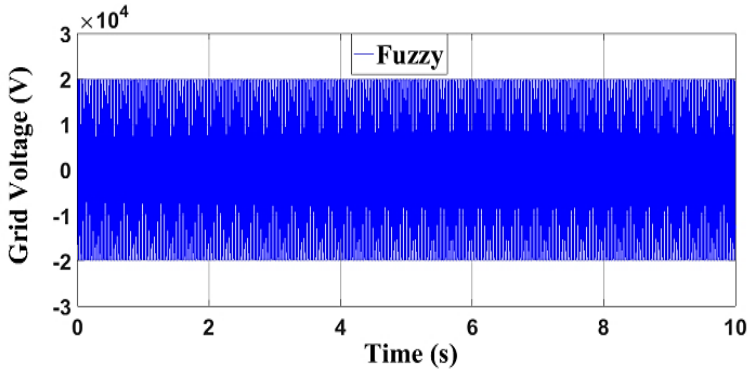

(a)

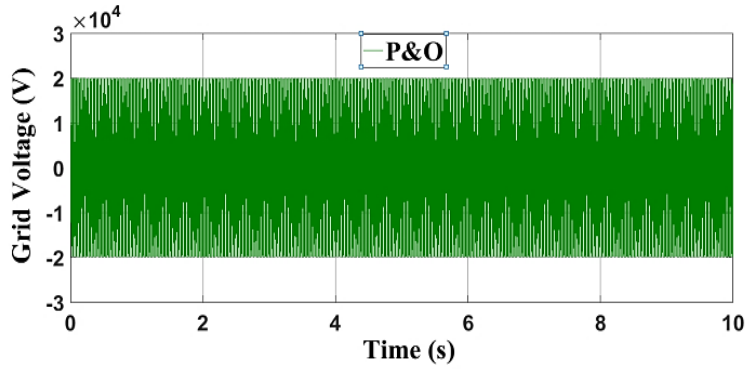

(b)

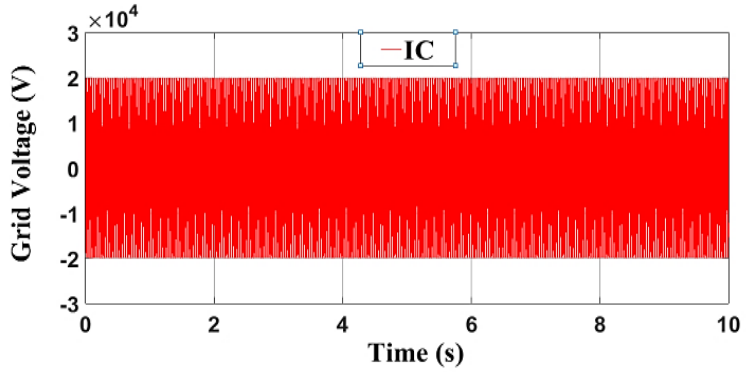

(c)

Figure 13. Grid voltage under different algorithms.

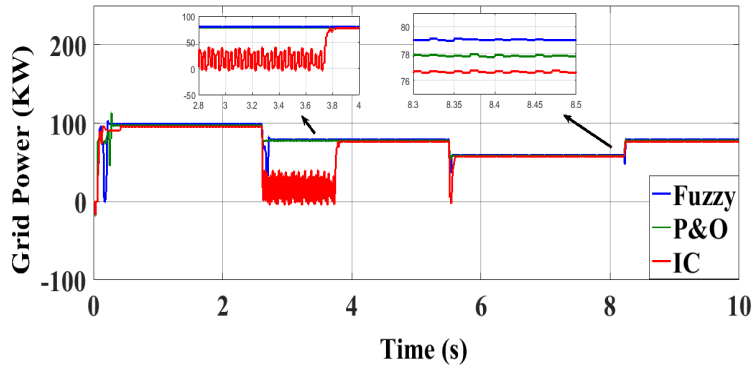

Figure 14. Grid power under different algorithms.

Table 4. Grid output power under different radiation

Time (sec)	Solar Radiation (W/m^2)	Grid Output power (KW)		
		IC MPPT	P&O MPPT	Fuzzy MPPT
1 to 2.6	1000	95.74	97.25	98.77
2.6 to 5.5	800	76.69	77.85	79.08
5.5 to 8.2	600	57.31	58.24	59.14
8.2 to 10	800	76.69	77.85	79.08

B. Results under ramp changes of solar radiation

Figure 15 presents the variations in sun-based radiation under the ramp profile with the steady surrounding temperature, as sun-oriented radiation beginning from 1000 W/m^2 was bit by bit decrease radiation to 800 W/m^2 and afterward decrease radiation until 600 W/m^2. At long last come back to 800 W/m^2. Figure 16 displays, PV yield framework execution correlation with IC, P&O and FLC technique under ramp variations of sun-oriented radiation. The yield of PV power in the three various procedures displays that the best yield power utilizing the FLC strategy contrasted with another strategy IC and P&O method. Likewise, by contrasting the FLC Technique execution and traditional P&O in the quick differing climate conditions of sunlight-based radiation, the FLC is more accurate than the traditional technique and under the high effectiveness, quick-shifting climate sun-powered radiation situations. The FLC keeps track of the optimum MPPT. The suggested FLC Technique for following the framework builds productivity than conventional innovation.

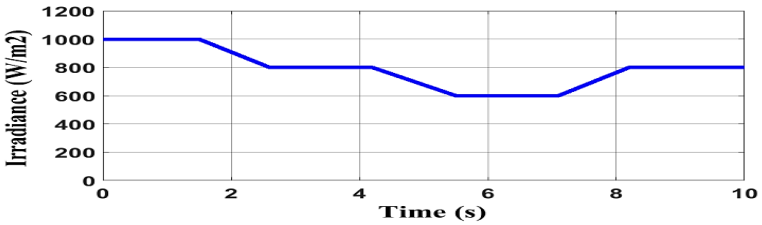

Figure 15. Irradiance in a ramp changed profile.

Figure 16 (a) illustrate the PV output voltage at different MPPT algorithms, showing that the best output voltage using FLC compared to IC and P&O schemes. By contrasting of yield the PV current of the three strategies as clarified in Figure 16 (b), FLC Technique is the most ideal exhibition to follow the limit of PV current. Figure 16 (c) presents the PV yield power in the three various strategies, indicating that the best yield power utilizing FLC compared to another technique IC and P&O. The framework motions are decreased about the MPP and the framework reaction is lower than the IC and P&O techniques. Figure 17, illustrate the generated active power to the utility grid.

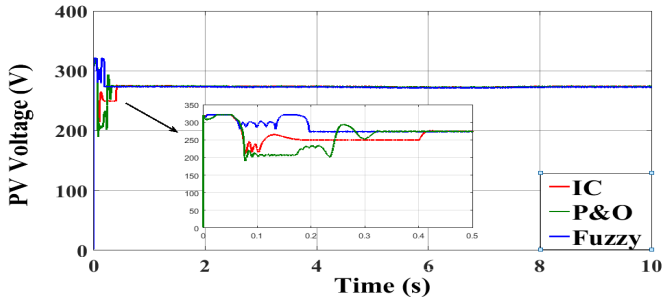

(a)

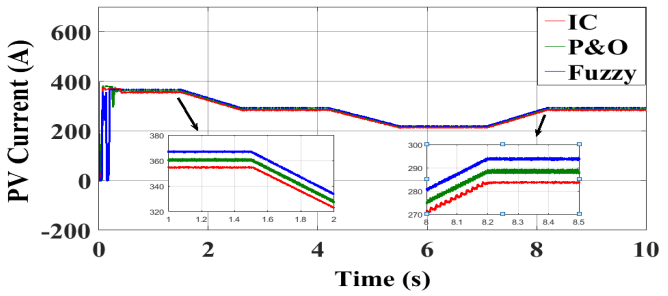

(b)

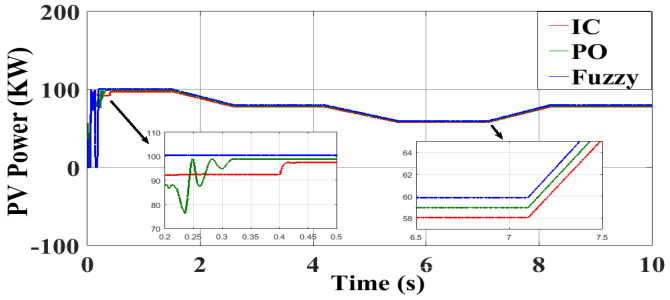

(c)

Figure 16. Performance comparison of PV system under ramp change irradiance; (a) output of PV voltage (b) output of PV current, and (c) output of PV power.

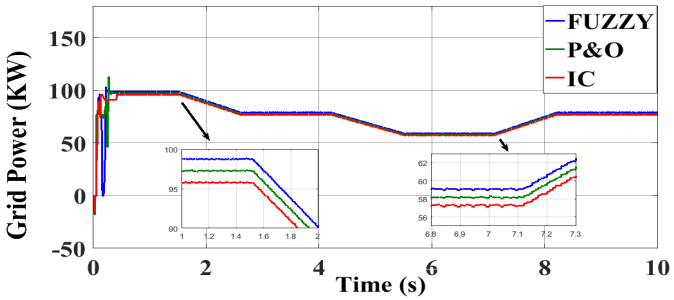

Figure 17. Grid power under different algorithms.

C. Results under random changes of solar radiation

Figure 18, shows the change of solar radiation under the random profile with constant ambient temperature. Figure 19, shows the PV output system performance comparison to IC, P&O, and FLC method at random changes in solar radiation. The output of PV power in the three different techniques shows that the best output energy using the FLC technique compared to another methods IC and P&O technique. Also, by comparing the FLC algorithm performance with traditional P&O in the fast-varying weather environments of solar radiation, the FLC is more accurate than the traditional method and under the high efficiency fast varying weather solar radiation environments. The FLC follows the best MPPT. The proposed FLC Technique for tracking the system increases efficiency than traditional technology.

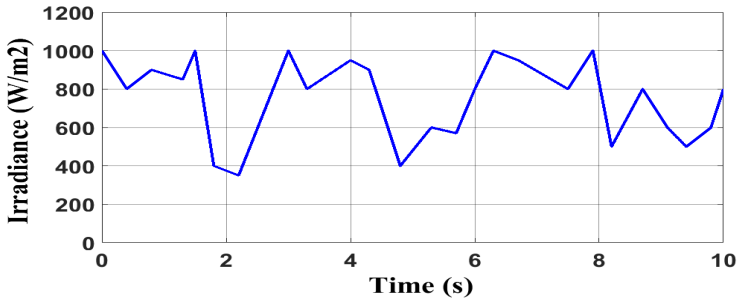

Figure 18. Irradiance in a randomly changed profile

Figure 19 (a) shows PV output voltage with three different MPPT methods. Consequently, the FLC scheme is the best performance of voltage output compared anther algorithms. By comparing of output the PV current of the three techniques as cleared in Figure 19(b), FLC Technique is the best performance to track the maximum possible of PV current. Figure 19 (c) shows the PV output power in the three different techniques, showing that the best output energy using FLC compared to the IC algorithm and P&O techniques. The system oscillations are reduced about the MPP and the system response is less than the IC and P&O algorithm. Good agreement between the PV power and grid power as showing in Figure 20.

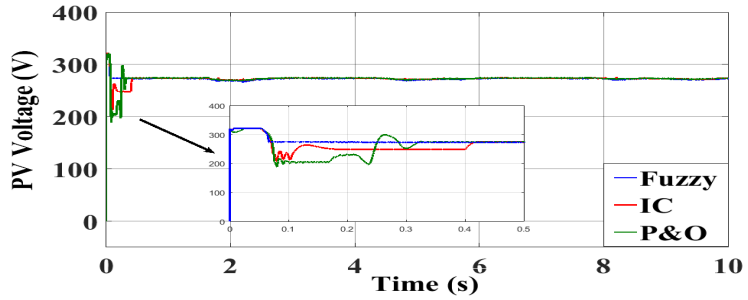

(a)

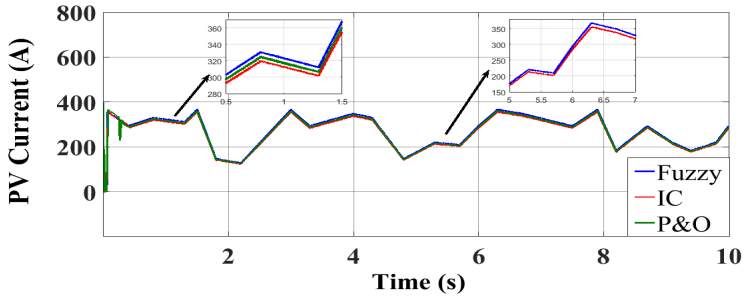

(b)

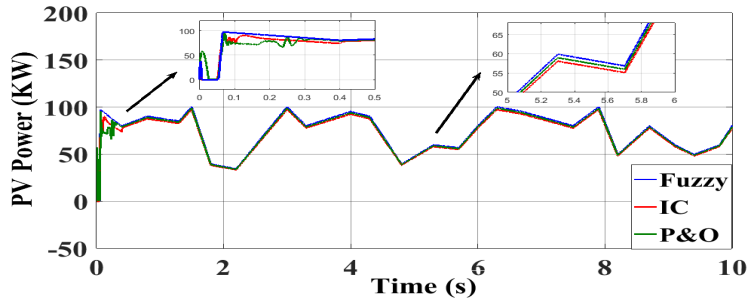

(c)

Figure 19. Performance comparison of PV system under random change irradiance; the output of PV voltage (b) output of PV current, and (c) output of PV power.

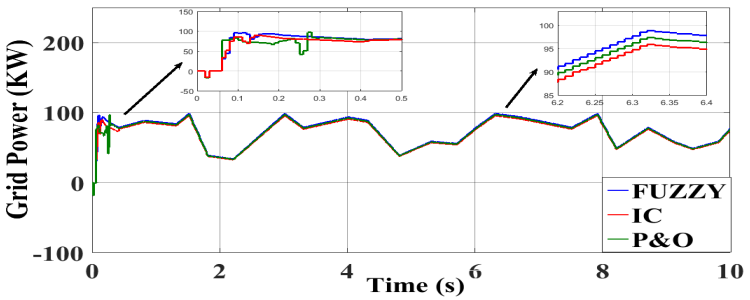

Figure 20. Grid power under different algorithms.

5. Experimental Setup of on-grid PV Systems

Figure 21 presents the schematic diagram of the PV systems connected to the grid. And Figure 22 shows an experimental set-up of grid-connected PV systems, which consists of power

supply, three-phase transformer, multimeter, and three-phase DC to AC inverter, each component will be specifications in details Table 5.

In the laboratory, the PV system action is simulated by the power supply test stand and PVSim software, the power supply that is used for Photovoltaic array simulation, the inverter is a device whose function is to convert the DC power from solar panels to AC power. To operate household appliances or pumps or connect the solar system to the national electricity grid, transformer is most preferred for grid connected PV generation system due to higher efficiency and lower cost, multimeters are tools used to measure current, voltage and resistance. Digital multimeters are much easier to read and provide more accurate readings. The digital multimeter displays the reading in digits most times on a LCD screen. This makes it possible to reproduce the conditions prevailing at real PV power system. As shown in Figure 22.

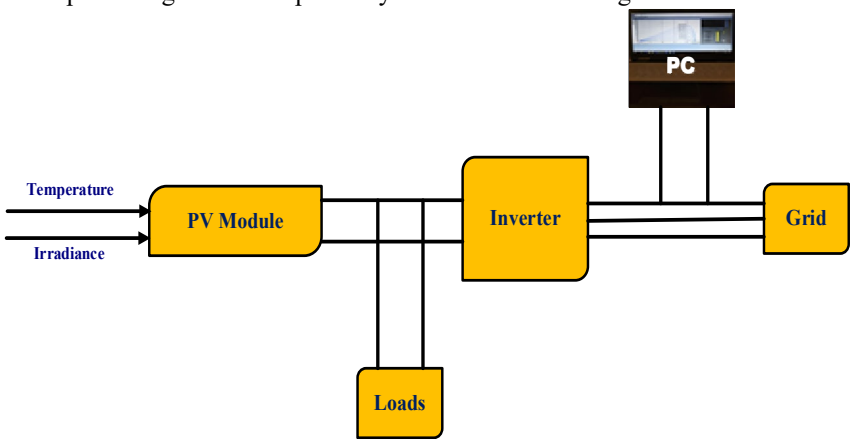

Figure 21. Schematic diagram of a PV systems connected to the grid.

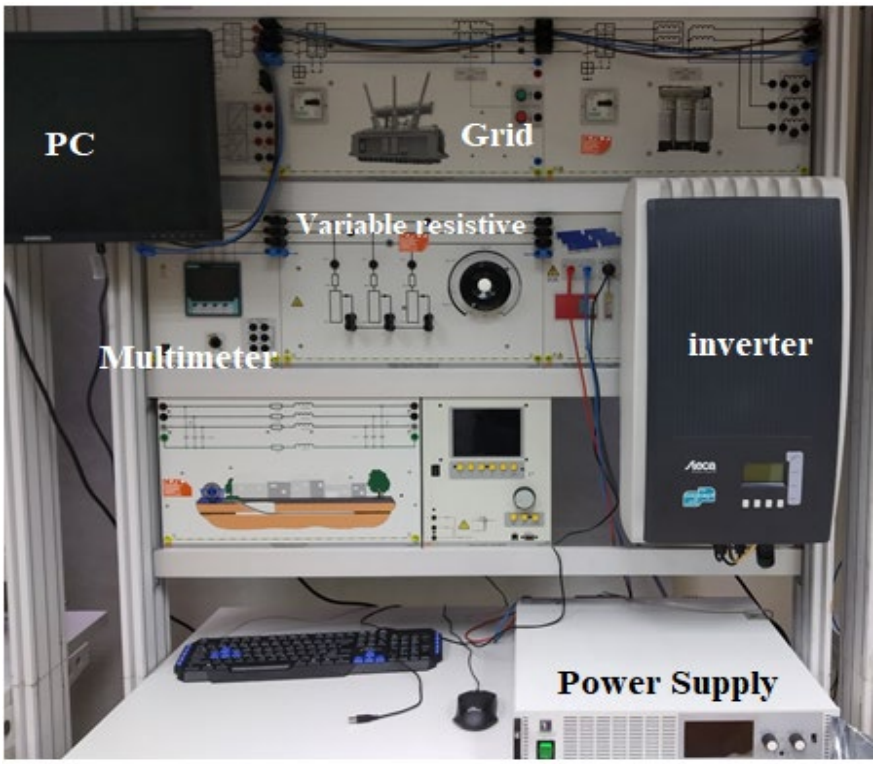

Figure 22. Experimental setup for the grid-connected PV system.

Table 5. Experimental Setup Parameters

Name of device	Parameters		value	
PV source	Output Voltage		500 V	
	Output Current		0 – 10 A	
	Power Rating		0 – 1500 W	
	Minimum Temperature		0° C	
	Maximum Temperature		50° C	
ON-grid inverter	DC Input		AC Output	
	Voltage	250 –1000 V	Voltage	3×230 V, 50-60 HZ
	MPP Voltage	300 - 800 V	P.F	0.8 – 1.0
	Max. Current	11 A		7 A
	IS.C max	13–20 A	Max. power	3200 W 3200 W
Three-phase transformer	Primary Voltage		3 x up to 400 V	
	Secondary Voltage		3x 0 ... 450 V	
	Nominal Power		1000 VA	
	Frequency		50/60 HZ	

6. Experimental Results

A. Performance of PV Array

The efficiency of a PV system is directly affected by the intensity of sun radiation and ambient temperature. The nonlinear I-V and P-V characteristic of the PV array with constant solar radiation equal 1000 W/m^2 is shown in Figure 23. For a constant temperature and different solar radiations (200:1000 W/m^2), the P-V and I-V characteristic are shown in Figure 24 and Figure 25. From Figure 24, it can be easily realized that as the solar radiation increases, the maximum power generation increases. Similarly, in Figure 25, it is observed that as the solar radiation increases, the PV module output current increases.

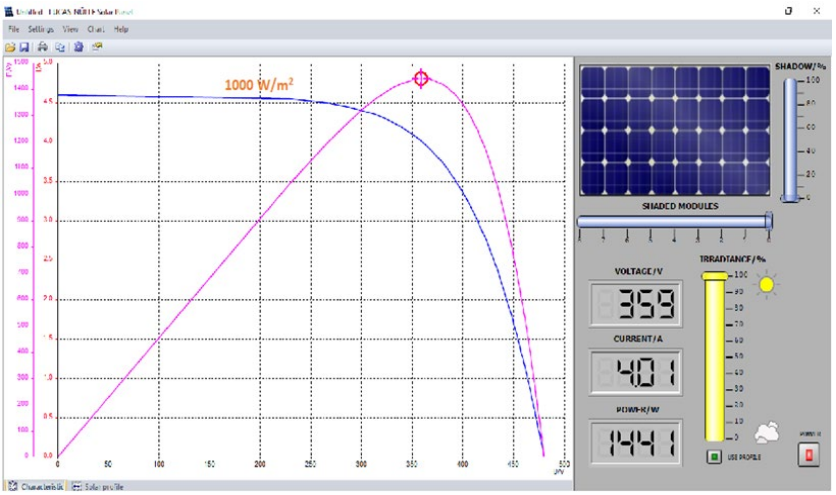

Figure 23. I-V and P-V characteristics of PV array with constant solar radiation 1000 W/m^2.

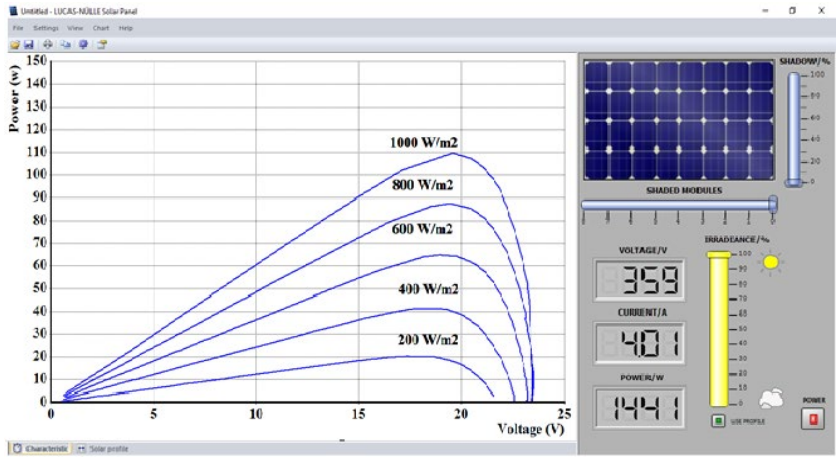

Figure 24. P-V curves of PV array with different solar radiations.

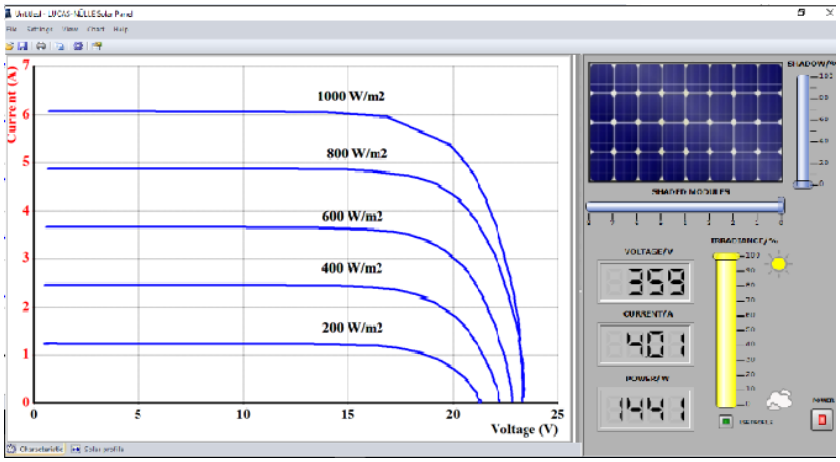

Figure 25. I-V curves of PV array with different solar radiations.

Figure 26, illustrates the variation of solar radiation, as seen in Figure 27, the PV generation power, current, and voltage. From the results, we see with the presence of the controller that the PV array is maintained to the best track of the maximum power. The PV voltage with the controller is constant with variation from solar radiation and good agreement between the PV power and PV current with solar radiation profile. As consequence, the MPPT with the controller is achieved.

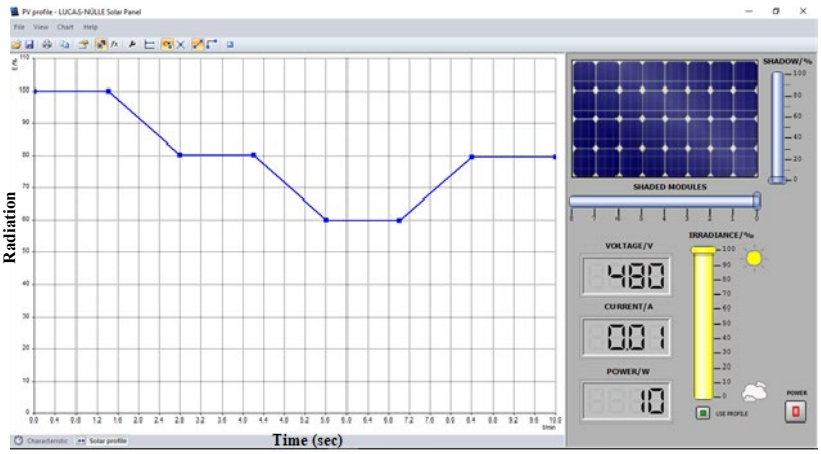

Figure 26. Variation of solar radiation.

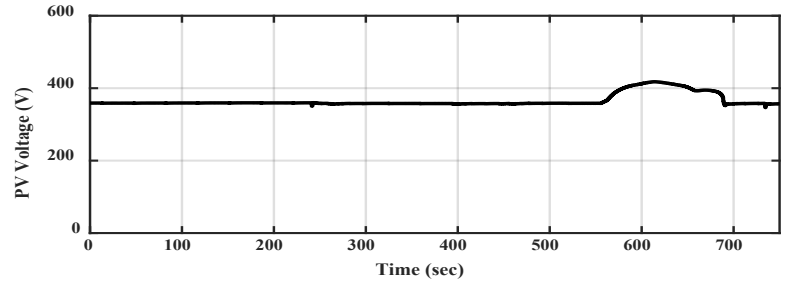

(a)

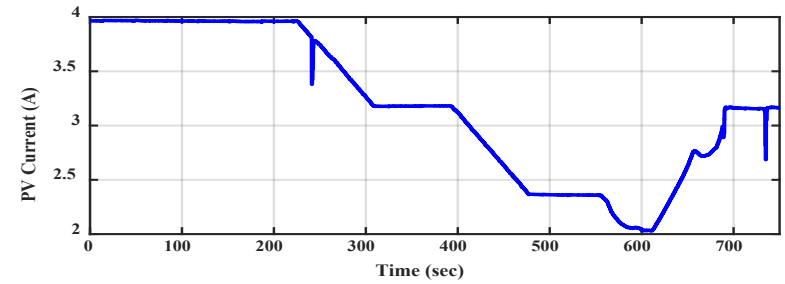

(b)

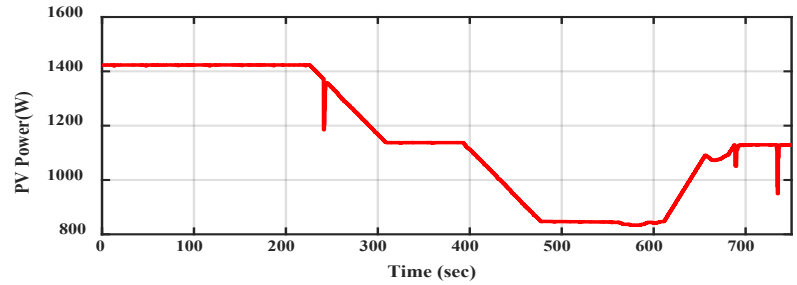

(c)

Figure 27. (a) Voltage, (b) Current and (c) Output Power of PV System

B. Performance of Grid Connected PV Systems

Figure 28, shows sample results of the R.M.S values of AC output voltage and current waveform of the grid connection with the controller. From the results, the grid connection better performs with the presence of the controller. The simulation waveform of a tracking process shows the impacts of the environmental conditions on the PV module performance during ramp changes of irradiance.

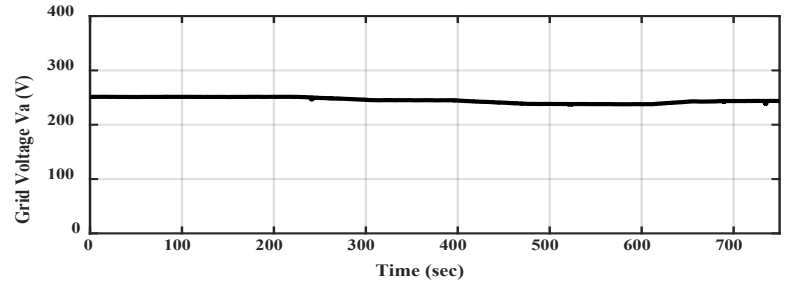

(a)

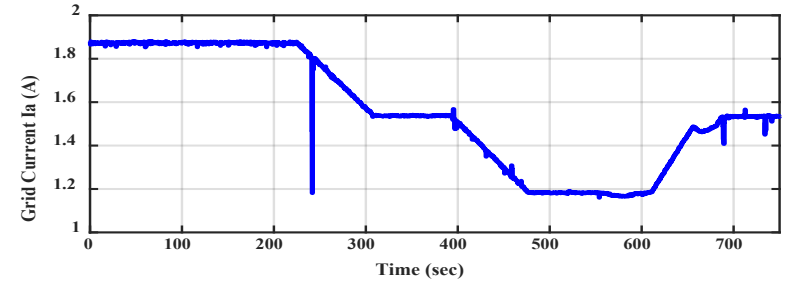

(b)

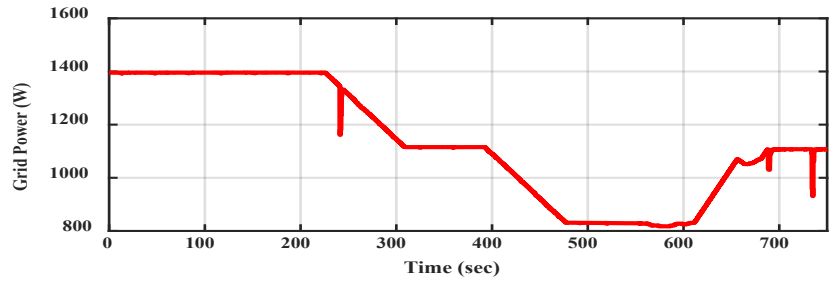

(c)

Figure 28. (a) AC Output Voltage, (b) Current and (c) Power Waveform with Grid Connection.

As shown in Figure 29, the experimental result has a maximum efficiency of grid-connected PV systems.

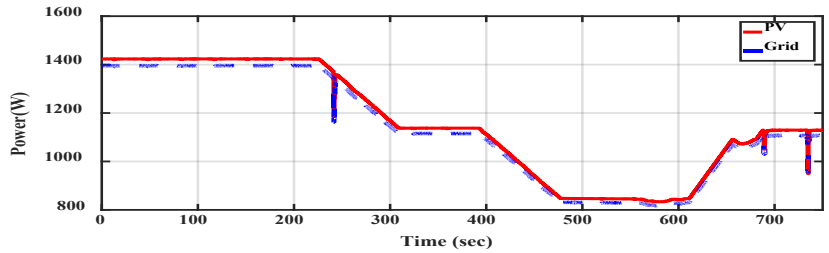

Figure 29. PV and grid power

From previous results, there is a good agreement between the experimental results and the simulation results for dynamic response at ramp changes of solar radiation.

7. Conclusions

This paper presents a complete exhibiting of the PV system with the control structures in the MATLAB /SIMULINK environment. The proposed control scheme based on the FLC technique is presented to improve the performance of MPPT of the grid-connected PV system. The proposed FLC technique is used to improve the system response and reduce the constant oscillations of the voltages, currents, and power, which improves the efficiency of the system. By comparing the FLC method and the P&O and IC method under different weather conditions the FLC was better for an average rate of maximum electric energy. The current-voltage curve method is used to separate environmental effects from affecting the working point to MPP in the case of continuous irradiation, most of the time. The proposed system works under different sectors with different steps to obtain the maximum capacity of solar energy and connected it with the grid. Finally, simulation results show the robustness and feasibility of the control scheme built on the proposed FLC technique for MPPT and increase efficiency. The simulation and experimental results show the robustness and feasibility of the control schemes. From the results, there is a good agreement between the experimental results and the simulation results for dynamic response at ramp changes of solar radiation.

8. References

[1]. M. R. Mostafa, N. H. Saad, and A. A. El-sattar, “Tracking the maximum power point of PV array by sliding mode control method,” *Ain Shams Eng. J.*, vol. 11, no. 1, pp. 119–131, 2020, doi: 10.1016/j.asej.2019.09.003.

[2]. P. Sivakumar, A. Abdul Kader, Y. Kaliavaradhan, and M. Arutchelvi, “Analysis and enhancement of PV efficiency with incremental conductance MPPT technique under non-linear loading conditions,” *Renew. Energy*, vol. 81, pp. 543–550, 2015.

[3]. S. S. Dessouky, S. A. M. Abdelwahab, W. S. E. Abdellatif, and M. A. Ali, “Performance enhancement of grid connected PV system by using ICMPPT technique,” Journal of Scientific and Engineering Research, vol. 5, no. 3, pp. 271-279, 2018.

[4]. J. H. Lee, H. Bae, and B. H. Cho, “Advanced incremental conductance MPPT algorithm with a variable step size,” in *2006 12th International Power Electronics and Motion Control Conference*, 2006, pp. 603–607.

[5]. G.-C. Hsieh, H.-I. Hsieh, C.-Y. Tsai, and C.-H. Wang, “Photovoltaic power-increment-aided incremental-conductance MPPT with two-phased tracking,” *IEEE Trans. Power Electron.*, vol. 28, no. 6, pp. 2895–2911, 2012.

[6]. P. Sivakumar, A. A. Kader, Y. Kaliavaradhan, and M. Arutchelvi, “Analysis and enhancement of PV efficiency with incremental conductance MPPT technique under non-linear loading conditions,” *Renew. Energy*, vol. 81, pp. 543–550, 2015.

[7]. N. Femia, G. Petrone, G. Spagnuolo, and M. Vitelli, “Optimization of perturb and observe maximum power point tracking method,” *IEEE Trans. power Electron.*, vol. 20, no. 4, pp. 963–973, 2005.

[8]. A. K. Abdelsalam, A. M. Massoud, S. Ahmed, and P. N. Enjeti, “High-performance adaptive perturb and observe MPPT technique for photovoltaic-based microgrids,” *IEEE Trans. power Electron.*, vol. 26, no. 4, pp. 1010–1021, 2011.

[9]. S. A. M. Abdelwahab, A. M. Hamada, and W. S. E. Abdellatif, " Comparative Analysis of the Modified Perturb & Observe with Different MPPT Techniques for PV Grid Connected Systems", I*nternational Journal of Renewable Energy Research*, vol.10, no.1, March, 2020.

[10]. K. Sundareswaran, V. Vignesh kumar, and S. Palani, “Application of a combined particle swarm optimization and perturb and observe method for MPPT in PV systems under partial shading conditions,” *Renew. Energy*, vol. 75, pp. 308–317, 2015.

[11]. Z. M. Ali, N. Vu Quynh, S. Dadfar, and H. Nakamura, "Variable step size perturb and observe MPPT controller by applying θ-modified krill herd algorithm-sliding mode controller under partially shaded conditions," *J. Clean. Prod.*, vol. 271, p. 122243, 2020.
[12]. W. Xiao and W. G. Dunford, "A modified adaptive hill climbing MPPT method for photovoltaic power systems," in *2004 IEEE 35th annual power electronics specialists conference (IEEE Cat. No. 04CH37551)*, 2004, vol. 3, pp. 1957–1963.
[13]. M. I. Bahari, P. Tarassodi, Y. M. Naeini, A. K. Khalilabad, and P. Shirazi, "Modeling and simulation of hill climbing MPPT algorithm for photovoltaic application," in *2016 International Symposium on Power Electronics, Electrical Drives, Automation and Motion (SPEEDAM)*, 2016, pp. 1041–1044.
[14]. M. Lasheen and M. Abdel-Salam, "Maximum power point tracking using Hill Climbing and ANFIS techniques for PV applications: A review and a novel hybrid approach," *Energy Convers. Manag.*, vol. 171, pp. 1002–1019, 2018.
[15]. H.-D. Liu, C.-H. Lin, K.-J. Pai, and Y.-L. Lin, "A novel photovoltaic system control strategies for improving hill climbing algorithm efficiencies in consideration of radian and load effect," *Energy Convers. Manag.*, vol. 165, pp. 815–826, 2018.
[16]. C. B. N. Fapi, P. Wira, M. Kamta, A. Badji, and H. Tchakounte, "Real-time experimental assessment of Hill Climbing MPPT algorithm enhanced by estimating a duty cycle for PV system," *Int. J. Renew. Energy Res.*, 2019.
[17]. H. Rezk *et al.*, "A novel statistical performance evaluation of most modern optimization-based global MPPT techniques for partially shaded PV system," *Renew. Sustain. Energy Rev.*, vol. 115, p. 109372, 2019.
[18]. N. Aouchiche, M. S. Aitcheikh, M. Becherif, and M. A. Ebrahim, "AI-based global MPPT for partial shaded grid connected PV plant via MFO approach," *Sol. Energy*, vol. 171, pp. 593–603, 2018.
[19]. H. Rezk and A. Fathy, "Simulation of global MPPT based on teaching--learning-based optimization technique for partially shaded PV system," *Electr. Eng.*, vol. 99, no. 3, pp. 847–859, 2017.
[20]. F. Liu, Y. Kang, Y. Zhang, and S. Duan, "Comparison of P&O and hill climbing MPPT methods for grid-connected PV converter," in *2008 3rd IEEE Conference on Industrial Electronics and Applications*, 2008, pp. 804–807.
[21]. P. Sahu, A. Sharma, and R. Dey, "Ripple Correlation Control Maximum Power Point Tracking for Battery Operated PV Systems: A Comparative analysis," in *2020 IEEE International IOT, Electronics and Mechatronics Conference (IEMTRONICS)*, 2020, pp. 1–6.
[22]. H. Attia, "High performance PV system based on artificial neural network MPPT with PI controller for direct current water pump applications," *Int. J. Power Electron. Drive Syst.*, vol. 10, no. 3, p. 1329, 2019.
[23]. A. M. Farayola, A. N. Hasan, and A. Ali, "Efficient photovoltaic MPPT system using coarse gaussian support vector machine and artificial neural network techniques," *Int. J. Innov. Comput. Inf. Control*, vol. 14, no. 1, 2018.
[24]. S. Assahout, H. Elaissaoui, A. El Ougli, B. Tidhaf, and H. Zrouri, "A neural network and fuzzy logic based MPPT algorithm for photovoltaic pumping system," *Int. J. Power Electron. Drive Syst.*, vol. 9, no. 4, p. 1823, 2018.
[25]. H. Li, D. Yang, W. Su, J. Lü, and X. Yu, "An overall distribution particle swarm optimization MPPT algorithm for photovoltaic system under partial shading," *IEEE Trans. Ind. Electron.*, vol. 66, no. 1, pp. 265–275, 2018.
[26]. R. B. A. Koad, A. F. Zobaa, and A. El-Shahat, "A novel MPPT algorithm based on particle swarm optimization for photovoltaic systems," *IEEE Trans. Sustain. Energy*, vol. 8, no. 2, pp. 468–476, 2016.
[27]. M. Mao, L. Zhang, Q. Duan, O. J. K. Oghorada, P. Duan, and B. Hu, "A two-stage particle swarm optimization algorithm for MPPT of partially shaded PV arrays," *Int. J. Green Energy*, vol. 14, no. 8, pp. 694–702, 2017.

[28]. A. Badis, M. N. Mansouri, and M. H. Boujmil, "A genetic algorithm optimized MPPT controller for a PV system with DC-DC boost converter," in *2017 International Conference on Engineering & MIS (ICEMIS)*, 2017, pp. 1–6.
[29]. M. S. R. Kumar, A. Amudha, and R. Rajeev, "Optimization For A Novel Single Switch Resonant Power Converter Using Ga To Improve Mppt Efficiency Of Pv Applications," *Int. J. Appl. Eng. Res.*, vol. 11, no. 9, pp. 6485–6488, 2016.
[30]. S. C. Wang, H. Y. Pai, G. J. Chen, and Y. H. Liu, "A Fast and Efficient Maximum Power Tracking Combining Simplified State Estimation with Adaptive Perturb and Observe," *IEEE Access*, vol. 8, pp. 155319–155328, 2020.
[31]. P. K. Pathak, A. Kumar Yadav, and P. A. Alvi, "Maximum Power Operation of SPV System using Advanced FL based Control Strategy," *2019 8th Int. Conf. Power Syst. Transit. Towar. Sustain. Smart Flex. Grids, ICPS 2019*, 2019.
[32]. L. Farah, A. Hussain, A. Kerrouche, C. Ieracitano, J. Ahmad, and M. Mahmud, "A highly-efficient fuzzy-based controller with high reduction inputs and membership functions for a grid-connected photovoltaic system," *IEEE Access*, vol. 8, pp. 163225–163237, 2020.
[33]. A. I. M. Ali, M. A. Sayed, and E. E. M. Mohamed, "Modified efficient perturb and observe maximum power point tracking technique for grid-tied PV system," *Int. J. Electr. Power Energy Syst.*, vol. 99, no. November 2017, pp. 192–202, 2018.
[34]. Y. Errami, M. Hilal, M. Benchagra, M. Maaroufi, and M. Ouassaid, "Nonlinear control of MPPT and grid connected for wind power generation systems based on the PMSG," in *2012 International Conference on Multimedia Computing and Systems*, 2012, pp. 1055–1060.
[35]. M. Mokhlis, M. Ferfra, H. A. Vall, R. El Idrissi, C. C. Ahmed, and A. Taouni, "Comparative study between the different MPPT techniques," *2020 5th Int. Conf. Renew. Energies Dev. Countries, REDEC 2020*, pp. 0–5, 2020.
[36]. X.-Z. Wang and C.-R. Dong, "Improving Generalization of Fuzzy IF--THEN Rules by Maximizing Fuzzy Entropy," *IEEE Trans. fuzzy Syst.*, vol. 17, no. 3, pp. 556–567, 2008.
[37]. H. Ying, "Conditions for general Mamdani fuzzy controllers to be nonlinear," in *2002 Annual Meeting of the North American Fuzzy Information Processing Society Proceedings. NAFIPS-FLINT 2002 (Cat. No. 02TH8622)*, 2002, pp. 201–203.
[38]. T. A. Runkler, "Extended defuzzification methods and their properties," in *Proceedings of IEEE 5th international fuzzy systems*, 1996, vol. 1, pp. 694–700.
[39]. H. Weihua, Z. Zheng, and F. Kangling, "Analysis and design of fuzzy-PID controller with generalized linear membership function," in *The 26th Chinese Control and Decision Conference (2014 CCDC)*, 2014, pp. 2365–2369.
[40]. M. Unde, K. Deokar, M. Hans, and S. Kawthe, "Closed-Loop Design of Fuzzy Logic Controller in Solar Power Generation," *Proc. 4th Int. Conf. Inven. Syst. Control. ICISC 2020*, no. Icisc, pp. 215–219, 2020.

Walid S.E. Abdellatif was born in Kafr-Elsheikh, Egypt. He received the B.Sc. Degree in Industrial Education from the Suez Canal University, Suez, Egypt, in 2006. He received the Master of Industrial Education degree in Electrical Power & Machines from Suez Canal University, Suez, Egypt, in 2012, and Ph.D. from Faculty of Industrial Education, Electrical Department, Suez University, Egypt, in 2016. He is an Assistant Professor in Electricity Department (Electrical Power &Machines), Faculty of Technology and Education, Suez University, Suez, Egypt form 2016. His research interests include renewable energy sources especially the wind energy issues, power electronics, micro grid and power quality.

Mohamed Saad Mohamed was born in Beheira, Egypt. He received the B.Sc. Degree in Industrial Education from Beni-Suef University, Beni-Suef, Egypt, in 2017. He is now Instructor in Process Control Technology Department, Faculty of Industrial Education, Beni-Suef University, Beni-Suef, Egypt form 2018. His research interests include renewable energy sources especially the PV energy issues, power electronics, micro grid and power quality.

Shimaa Barakat was born in Fayoum, Egypt in 1980. She received the B.S., M.S. and Ph.D. degrees in electrical engineering from Fayoum University, in 2002, 2014 and 2018. Her research interests include renewable energy, which includes solar, wind and biomass, as well as fuel cells, she also interested in the application of optimization techniques in renewable energy systems.

Ayman Mohamed Moftah Brisha was born in Gharbia, Egypt. He received the Master Degree candidate in Eindhoven Technical University (ETU), NL, in 1998. Lecturer At Industrial Education College (IEC) Beni_Suef University Feb.1998 – Nov. 2001. PHD candidate at Moscow power Engineering Institute (MPEI) (Technical University (TU) Nov. 2001 – 1 April 2005. Assistant Professor College of Industrial Education –Beni Suef University (ARE), Beni-Suef, ARE April, 2005 – August 2006. Assistant Professor, Taibah University, AL_Madinah Al-Munawarrah KSA August 2006 – August 2012. Assistant Professor, Beni Suef University, Beni Suef - ARE Oct. 2012 – Now. His research interests include Computer Science Engineering, Systems and Computer Engineering.